Chiral Stilbazolium Chromophores: An Approach toward Multiproperty Materials Combining Conductivity and Second-Order Optical Nonlinearities

Raquel Andreu, Isabelle Malfant, Pascal G. Lacroix,* and Heinz Gornitzka

Laboratoire de Chimie de Coordination du C.N.R.S. 205 Route de Narbonne, 31077 Toulouse, France

Keitaro Nakatani

P.P.S.M., Ecole Nationale Supérieure de Cachan, Avenue du Président Wilson, 94235 Cachan, France

Received November 5, 1998

A new chiral cyanine dye, 4′-[2-(methoxymethyl)pyrrolidinyl]-1-methylstilbazolium iodide ($MPMS^+I^-$) is reported. It crystallizes in the monoclinic $P2_1$ space group. $a = 16.559(2)$ Å, $b = 6.263(1)$ Å, $c = 24.477(3)$ Å, $\beta = 109.20(1)°$, $Z = 2$. The hyperpolarizability of $MPMS^+I^-$ is compared versus that of 4′-dimethylamino-1-methylstilbazolium iodide ($DAMS^+I^-$). $MPMS^+I^-$ is phase matchable and exhibits an efficiency up to 80 times that of urea in second-harmonic generation (SHG). Both compounds (C^+I^-) react with tetracyanoquinodimethane (TCNQ), and the resulting $C^+(TCNQ_2)^-$ exhibit conductivities in the range 10^{-3}−10^{-2} S cm^{-1}. The possibility of combining conductivity and optical nonlinearities is discussed.

Introduction

Molecular materials are a promising class of new materials that have emerged in many area of material science for designing new magnets,[1,2] molecular assemblies for data storage,[3] nonlinear optical (NLO) materials,[4,7] conductors, and superconductors.[8−10] The versatility of molecular chemistry offers a unique opportunity to meet additional challenges, such as designing multifunctional materials that would simultaneously possess several properties. Multifunctional molecular materials are of growing interest, because they should offer the possibility to manipulate one property by using another one. For example, it has recently been reported that a magnetic field could restore a metallic state in a paramagnetic conductor.[11] Materials combining magnetism[12,13] or conductivity[14,15] with NLO properties have already been reported. Beside the possibility of interaction between different properties, these materials could also attract some interest in multidisciplinary technologies, where several properties need to be linked in the same device. Among them, the technology of optoelectronics integrates photonic devices with standard semiconductor electronics, to combine the information processing capabilities of electrons and the speed of the light, which makes the need for photonic−electronic compatible materials pressing.[16] NLO crystals such as $LiNbO_3$ are good candidates for photonics, but not easy to incorporate into electronic devices. On the other hand, silicon is the material of choice for semiconductor-based electronics, but it is not suitable for the implementation of optical functions such as light emission and modulation, although several strategies are being considered to realize Si-compatible optoelectronics.[16]

Few studies aiming at connecting NLO and conductivity in a molecular material have already been reported. Sutter has combined 7,7′,8,8′-tetracyanoquinodimethane (TCNQ) with NLO chromophore to obtain a material exhibiting photoconductivity and second-order nonlinearity,[14] and Alagesan has obtained a mixed valent organometallic molecule with large second-order

(1) Kahn, O. *Molecular Magnetism*; VCH: Weinheim 1993.
(2) Miller, J. S.; Epstein, A. J. *Angew. Chem., Int. Ed. Engl.* **1994**, *33*, 3, 385.
(3) Kahn, O.; Martinez, C. J. *Science* **1998**, *279*, 44.
(4) Optical Nonlinearities in Chemistry, a special issue of *Chem. Rev.* **1994**, *94 (Jan.)*.
(5) Prasad, P. N.; Williams, D. J. *Introduction to Nonlinear Optical Effects in Molecules and Polymers*; Wiley-Interscience: New York, 1991.
(6) Materials for Nonlinear Optics: Chemical Perspectives; Marder S. R., Sohn J. E., Stucky G. D. Eds., *ACS Symp. Ser.* **1991**, 455.
(7) Zyss J. *Molecular Nonlinear Optics*; Academic Press: New York, 1994.
(8) Cassoux, P.; Miller, J. S. In *Chemistry of Advanced Materials: An Overview*; Interrante, L. V., Hampden-Smith, M. J., Eds.; Wiley-VCH: New York, 1998; p 19.
(9) Special Issue on Molecular Conductors. *J. Mater. Chem.* **1995**, *5* (10).
(10) Williams, J. M.; Ferraro, J. R.; Thorn, R. J.; Carlson, K. D.; Geiser, U.; Wang, H. H.; Kini, A. M.; Whangbo, *Organic Superconductors (Including Fullerenes)*; Prentice Hall: Englewood Cliffs, NJ, 1992.
(11) Goze, F.; Laukhin, V. N.; Brossard, L.; Audouard, A.; Ulmet, J. P.; Askenazy, S.; Naito, T.; Kobayashi, H.; Kobayashi M.; Cassoux, P. *Europhys. Lett.* **1994**, *28*, 427.
(12) (a) Clément, R.; Lacroix, P. G.; O′Hare D.; Evans, J. *Adv. Mater.* **1994**, *6*, 794. (b) Lacroix, P. G.; Clément, R.; Nakatani, K.; Zyss J.; Ledoux, I. *Science* **1994**, *263*, 658.
(13) Bernard, S.; Yu, P.; Coradin, T.; Rivière, E.; Nakatani, K.; Clément, R. *Adv. Mater.* **1997**, *9*, 981.
(14) Sutter, K.; Hulliger J.; Günter, P. *Solid State Commun.* **1990**, *74*, 867.
(15) Lacroix P. G.; Nakatani, *Adv. Mater.* **1997**, *9*, 1105.
(16) Silicon-Based Optoelectronics, a special issue of *MRS Bull.* **1988**, *23*, 4.

10.1021/cm9810436 CCC: $18.00
Published on Web 02/04/1999

Chart 1

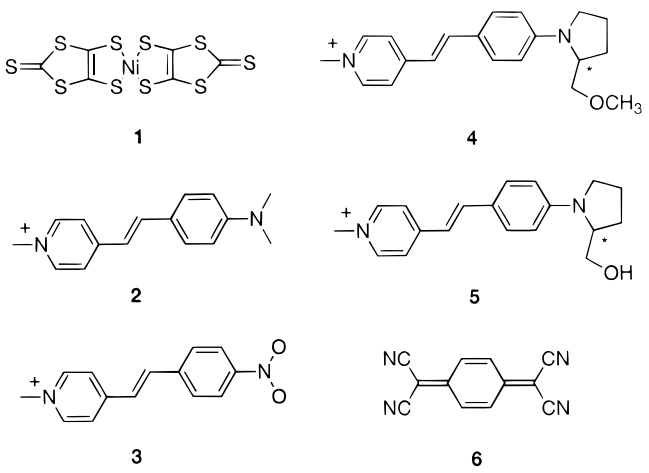

nonlinearity by oxidation with TCNQ.[17] Along this line, and as part of our general effort aimed at extending the range of molecular materials combining two properties in the same crystal, we have recently reported on the 1:1 salt made of nickel bis(dithiolene) metal complexes ($[Ni(dmit)_2]^-$ (**1**, Chart 1) and 4′-dimethylamino-1-methylstilbazolium, $DAMS^+$ (**2**).[18] The resulting 1:1 hybrid salt exhibits semiconductivity, but no NLO response, due to crystal centrosymmetry. This first report has raised two important prerequisites: (i) achieving an interplay between conductivity and NLO properties and (ii) observing a bulk nonlinearity in these hybrid salts.

(i) At first, it seems possible to link NLO and conductivity in a salt, as both properties deal with the same general concept of charge transfer: an intermolecular charge transfer along stacks of ions in conducting systems and an intramolecular charge transfer between a donor (D) and an acceptor (A) counterpart in NLO systems. The possibility of π-overlaps between the ions could modulate the overall electronic structure, which would be desirable for linking the properties. We have discussed this possibilitity in a second contribution, where 4′-nitro-1-methylstilbazolium, $NOMS^+$ (**3**), instead of $DAMS^+$ was combined with $[Ni(dmit)_2]^-$.[19] The electron rich $[Ni(dmit)_2]^-$ species were observed to strongly interact with $NOMS^+$ (a cation more reducible than $DAMS^+$), as evidenced by seven short distances (less than the sum of the van der Waals radii) between cationic and anionic species. In addition, we have pointed out that electron sharing between anions and cations could affect the magnitude and even the sign of the hyperpolarizability of the chromophores. Therefore, an adjustment in the redox potentials of the cations (C^+/C°) and the anions (A^-/A°) appears as the key in this research, where the interplay between light and electricity could be achieved through the modification of the molecular hyperpolarizability by applying a pulse of electric current.

The second issue (ii) raised by these hybrid structures is related to the possibility of recording observable bulk nonlinearities. A survey of the Cambridge Data Base reveals that only two structures based on $[Ni(dmit)_2]^-$ in more than 100 entries actually are noncentrosymmetric. The large size, centrosymmetric shape, and strong tendency for a two-dimensionnal S···S network observed in $[Ni(dmit)_2]^-$ can probably account for this structural feature, whatever the nature of the counteranion is.

In the present contribution, we wish to report on a strategy based on using chiral chromophores closely related to $DAMS^+$, namely 4′-[2-(methoxymethyl)pyrrolidinyl]-1-methylstilbazolium, $MPMS^+$ (**4**), with the aim of forcing the crystallization in a noncentrosymmetric space group, which is an important prerequisite for the observation of bulk second-order NLO properties. $MPMS^+$ has been preferred instead of the related 4′-[2-(hydroxymethyl)pyrrolidinyl]-1-methylstilbazolium, $HPMS^+$ (**5**), reported in a previous study[15] because of a better crystallinity. Contrary to $HPMS^+I^-$, which is an amorphous compound, $MPMS^+I^-$ crystallizes, and we present here its crystal structure. The molecular hyperpolarizability (β) of $MPMS^+$ will be discussed versus that of the well-known $DAMS^+$ chromophore, both experimentaly (optical spectroscopy) and theoretically, within the INDO/SOS formalism[20] on the basis of available crystal data. To overpass the tendency for centosymmetry observed in $[Ni(dmit)_2]^-$ salts, the smaller tetracyanoquinodimethane, TCNQ (**6**), has been used as the anionic counterpart, bringing about the NLO materials with additional conducting properties.

Experimental Section

Starting Materials and Equipment. Solvents (SDS, synthesis grade) were used as supplied. TCNQ, 4-dimethylaminobenzaldehyde, and 4-fluorobenzaldehyde were purchased from Aldrich Chimica and were used without further purification, except TCNQ, which was recrystallized in acetonitrile. 4-Picoline (Janssen Chimica) and (*R*)-(+)-2-(methoxymethyl)-pyrrolidine (Merck) were used as received. Elemental analysis were performed by the Service de Microanalyse du Laboratoire de Chimie de Coordination du C.N.R.S. IR spectra were recorded on a Perkin-Elmer 1725 X spectrometer, electronic spectra on a Shimadzu UV 3100 spectrophotometer, ^{1}H NMR on a Bruker AM 250 spectrometer, and EPR spectra, on a Bruker ER 200 D spectrometer. Thermal measurements were performed by TG/DTA analysis on a Setaram-TGDTA92 thermoanalyzer. The experiments were conducted under nitrogen on 5 mg of sample (rate of heating, 10 °C/min).

Synthesis and Characterization of Stilbazolium Salts. *N*-Methylstilbazolium iodide, $DAMS^+I^-$ (**2**), was readily synthesized by reaction of *N*-methylpicolinium iodide and the appropriate aldehyde following the procedure previously described.[21] The purity of the material was checked by ^{1}H NMR and UV−vis spectroscopies.[21,22] $MPMS^+I^-$ and $HPMS^+I^-$ have been synthesized following the same general route described below.

4′-[2-(Methoxymethyl)pyrrolidinyl]-1-methylstilbazolium iodide, $MPMS^+I^-$ (4). 4-[2-(Methoxymethyl)pyrrolidinyl]-benzaldehyde was prepared according to the route recently described:[23−25] to a solution of 2 mL (16.2×10^{-3} mol) of (*R*)-(+)-2-(methoxymethyl)pyrrolidine and 1.73 mL (16.2×10^{-3}

(17) Alagesan, K., Ray, P. C.; Das, P. K.; Samuelson, G. *Curr. Sci.* **1996**, *70*, 69.
(18) Malfant, I.; Andreu, R.; Lacroix, P. G.; Faulmann, C.; Cassoux, P. *Inorg. Chem.* **1998**, *37*, 3361.
(19) Malfant, I.; Cordente, N.; Lacroix, P. G.; Lepetit, C. *Chem. Mater.* **1998**, *10*, 4079.
(20) Kanis, D. R.; Ratner, M. A.; Marks, T. J. Ref 4, p 195.
(21) Kung, T. K. *J. Chin. Chem. Soc.* **1978**, *25*, 131.
(22) Marder, S. R.; Perry, J. W.; Yakymyshyn, C. P. *Chem. Mater.* **1994**, *6*, 1137.
(23) Tiemann, B. G.; Marder, S. R.; Perry, J. W.; Cheng, L. T. *Chem. Mater.* **1990**, *2*, 690.
(24) Zhao, C.; Park, C. K.; Prasad, P. N.; Zhang, Y.; Ghosal, S.; Burzynski, R. *Chem. Mater.* **1995**, *7*, 1237.

mol) of 4-fluorobenzaldehyde in dry DMSO (8 g) was added 3.35 g (24.3×10^{-3} mol) of K_2CO_3. The mixture was heated at 130 °C for 24 h under an argon atmosphere. After cooling, the resulting mixture was poured into 250 mL of water, extracted with CH_2Cl_2. Chromatography on SiO_2 using CH_2Cl_2−AcOEt (19/1) afforded 4-[2-(methoxymethyl)pyrrolidinyl]benzaldehyde as an orange oil (yield 80%). ^{1}H NMR ($CDCl_3$) δ 9.69 (s, 1 H), 7.70 (d, $J = 8.9$ Hz, 2 H), 6.64 (d, $J = 8.9$ Hz, 2 H), 4.08−3.97 (m, 1H), 3.50−3.44 (m, 2H), 3.35 (s, 3H), 3.26−3.17 (m, 2H), 2.08−1.99 (m, 4H). A mixture of 2.83 g of this oil (13×10^{-3} mol) and 3.05 g (13×10^{-3} mol) of 1-methylpicolinium iodide was refluxed overnight in 15 mL of 2-propanol with few drops of piperidine, according to the general procedure previously described.[21] After cooling, the red solid collected is recrystallized from methanol, to afford 2.77 g of $MPMS^+I^-$ (yield 48%). Anal. Calcd (found) for $C_{20}H_{25}IN_2O$: C, 55.05 (54.1); H, 5.78 (5.6); N, 6.42 (6.2).^{1}H NMR (DMSO-d_6) δ 8.80 (d, $J = 6.7$ Hz, 2 H), 8.16 (d, $J = 7.7$ Hz, 2 H), 8.03 (d, $J = 16.1$ Hz, 1 H), 7.71 (d, $J = 8.7$ Hz, 2 H), 7.27 (d, $J = 16.1$ Hz, 1 H), 6.81 (d, $J = 8.7$ Hz, 2 H), 4.29 (s, 3H), 4.10 (m, 1 H), 3.6−3.2 (m, 7 H), 2.07 (s, 4 H). Single crystals were obtained by slow diffusion of diethyl ether into a concentrated solution of $MPMS^+I^-$ in acetonitrile. $HPMS^+I^-$ (**5**) has been obtained accordingly, using (*S*)-(+)-2-pyrrolidinemethanol instead of (*R*)-(+)-2-(methoxymethyl)pyrrolidine. Anal. Calcd (found) for $C_{19}H_{23}IN_2O$: C, 54.04 (53.47); H, 5.49 (5.44); N, 6.64 (6.22).[15]

The TCNQ salts of $DAMS^+$ and $MPMS^+$ were synthesized under an inert atmosphere. **DAMS(TCNQ)$_2$.** $DAMS^+I^-$ (72 mg, 2×10^{-4} mol) in 40 mL of ethanol was transferred to a solution of TCNQ (80 mg, 4×10^{-4} mol) in the same volume of acetonitrile. After standing overnight at −15 °C, dark needles were filtered and washed with a small amount of cold acetonitrile. Anal. Calcd (found) for $C_{40}H_{27}N_{10}$: C, 74.17 (74.0); H, 4.20 (4.0); N, 21.63 (21.6). **MPMS(TCNQ)$_2$ and HPMS(TCNQ)$_2$** were synthesized in pure acetonitrile followed by slow evaporation in air, as a trend for precipitation of a small amount of $TCNQ^0$ was observed when experiments were conducted in ethanol and precipitations were achieved at low temperature. Anal. Calcd (found) for $MPMS(TCNQ)_2$ ($C_{44}H_{33}N_{10}O$): C, 73.62 (73.0); H, 4.63 (4.6); N, 19.52 (19.3). For $HPMS(TCNQ)_2$ ($C_{43}H_{31}N_{10}O$): C, 73.38(72.6); H, 4.44 (4.5); N, 19.91 (19.2).

X-ray Data Collection and Structure Determination. The data were collected at 180 K on a Stoe Imaging Plate Diffraction System (IPDS) equipped with an Oxford Cryosystems cooler device. The crystal-to-detector distance was 80 mm. 118 exposures (8 min per exposure) were obtained with $0 < \varphi < 200.6°$ and with the crystals rotated through 1.7° in φ. Owing to the rather low μx value (1.349 mm^{-1}), no absorption correction was considered. Details of the data collection and refinement are given in Table 1. The structure was solved by direct methods (SHELXS-97)[26] and 488 parameters using 195 restraints were refined using the least-squares method on F^2.[27] The absolute structure parameter is 0.17(12). All hydrogen atoms are refined with a riding model. A molecule of diethyl ether is refined anisotropically, ignoring the symmetry using PART-1 with the occupancy of 0.5 using ADP and distance restraints. A disorder of one methoxy group (O2−C40) is refined anisotropically on two positions with the occupancies of 0.56/0.44 using ADP and distance restraints.

Calculation of Molecular NLO Response. The all-valence INDO (intermediate neglect of differencial overlap) method,[28] in connection with the sum-over-state (SOS) formalism,[29] was employed. Details of the computationally efficient INDO-SOS-based method for describing second-order molecular optical nonlinearities have been reported elsewhere.[20] Calculation was performed using the INDO/1 Hamiltonian incorporated in the commercially available MSI software package INSIGHT II (4.0.0). The monoexcited configuration interaction (MECI) approximation was employed to describe the excited states. The 100 energy transitions between the 10 highest occupied molecular orbitals and the 10 lowest unoccupied ones were chosen to undergo CI mixing. Structural parameters used for the INDO calculations were taken from the present crystal study for $MPMS^+I^-$ (molecules 1 and 2) and from a previously reported structure for $DAMS^+I^-$.[30] Although, the environment of the chromophores has been reported to influence the β values in some cases,[31] the iodide that is present in both $MPMS^+I^-$ and $DAMS^+I^-$ crystal structures was not introduced in the calculations. The position of iodide above the plane of the pyridinium rings (vide infra) reveals the same local environment for $DAMS^+$ and $MPMS^+$.

Table 1. Data Collection and Refinement for $MPMS^+I^-\cdot{}^1/_4Et_2O\cdot{}^1/_2H_2O$

empirical formula	$C_{21}H_{28.5}IN_2O_{1.75}$
M_w	463.86
crystal color	red
crystal dimensions, mm	0.8 × 0.1 × 0.02
temperature, K	180
crystal system	monoclinic
space group	$P2_1$
a, Å	16.559(2)
b, Å	6.263(1)
c, Å	24.477(3)
β, deg.	109.20(1)
Z	2
d_{calc}, g·cm^{-1}	1.285
μ (MoKα), mm^{-1}	1.349
F(000)	942
diffractometer	IPds Stoe
radiation (MoKα), Å	0.71073
2θ range, deg.	$3.5 < 2\theta < 48.6$
scan type	ϕ
reflns collected	15596
unique reflns	5320
no. of parameters	488
GOF on F^2	0.944
R^a (for $F > 2(F)$)	0.0838
wR_2^b	0.2166

^{a} $R1 = ||F_o| - |F_c||/|F_o|$. ^{b} $wR_2 = (w(F_o^2 - F_c^2)^2/w(F_o^2)^2)^{1/2}$.

NLO Measurements. The second-order optical nonlinearities were investigated by second-harmonic generation (SHG). The measurements of SHG intensities were carried out by the Kurtz−Perry powder technique,[32] using a picosecond Nd:YAG pulsed (10 Hz) laser operating at $\lambda = 1.064$ μm. The outcoming Stokes-shifted radiation at 1.907 μm generated by Raman effect in a hydrogen cell was used as the fundamental beam for second-harmonic generation. The SHG signal was detected by a photomultiplier and recorded on an ultrafast Tektronic 7834 oscilloscope. For $MPMS^+I^-$, the measurements were performed on calibrated powder. For TCNQ salts, the SHG signals were recorded on pressed pellets to overcome problems related to the strong absorbance of TCNQ salts, following the method described in the litterature.[33]

Conductivity Measurements. In the absence of suitable single crystals, two probe measurements were carried out on pressed pellets of pure powder materials (size: 1 mm^2 × about 0.5 mm) obtained by careful grinding. The cylinders used to press the materials were used as electrodes.

(25) Serbutoviez, C.; Bosshard, C.; Knöpfle, G.; Wyss, P.; Prêtre, P.; Günter, P.; Schenk, K.; Solari, E.; Chapuis, G. *Chem. Mater.* **1995**, *7*, 1198.
(26) G. M. Sheldrick, Acta Crystallogr. **1990**, *A46*, 467.
(27) SHELXL-97, Program for Crystal Structure Refinement, G. M. Sheldrick, University of Göttingen, 1997.
(28) (a) Zerner, M.; Loew, G.; Kirchner, R.; Mueller-Westerhoff, U. *J. Am. Chem. Soc.* **1980**, *102*, 589. (b) Anderson, W. P.; Edwards, D; Zerner, M. C. *Inorg. Chem.* **1986**, *25*, 2728.
(29) Ward, J. F. *Rev. Mod. Phys.* **1965**, *37*, 1.
(30) Lu, T. H.; Lee, T. J.; Wong, C.; Kuo, K. T. *J. Chin. Chem.* **1979**, *26*, 53.
(31) (a) Di Bella, S.; Fragalà, I.; Ratner, M. A.; Marks, T. J. *Chem. Mater.* **1995**, *7*, 400. (b) Di Bella, S.; Marks, T. J.; Ratner, M. A. *J. Am. Chem. Soc.* **1994**, *116*, 6, 4440. (c) Di Bella, S.; Ratner, M. A.; Marks, T. J. *J. Am. Chem. Soc.* **1992**, *114*, 4, 5842.
(32) (a) Kurtz, S. K.; Perry, T. T. *J. Appl. Phys.* **1968**, *39*, 3798. (b) Dougherty, J. P.; Kurtz, S. K. *J. Appl. Crystallogr.* **1976**, *9*, 145.
(33) Bailey, R. T.; Blaney, S.; Cruickshank, F. R.; Guthrie, S. M. G.; Pugh, D.; Sherwood, J. N. *Appl. Phys.* **1988**, *B47*, 83.

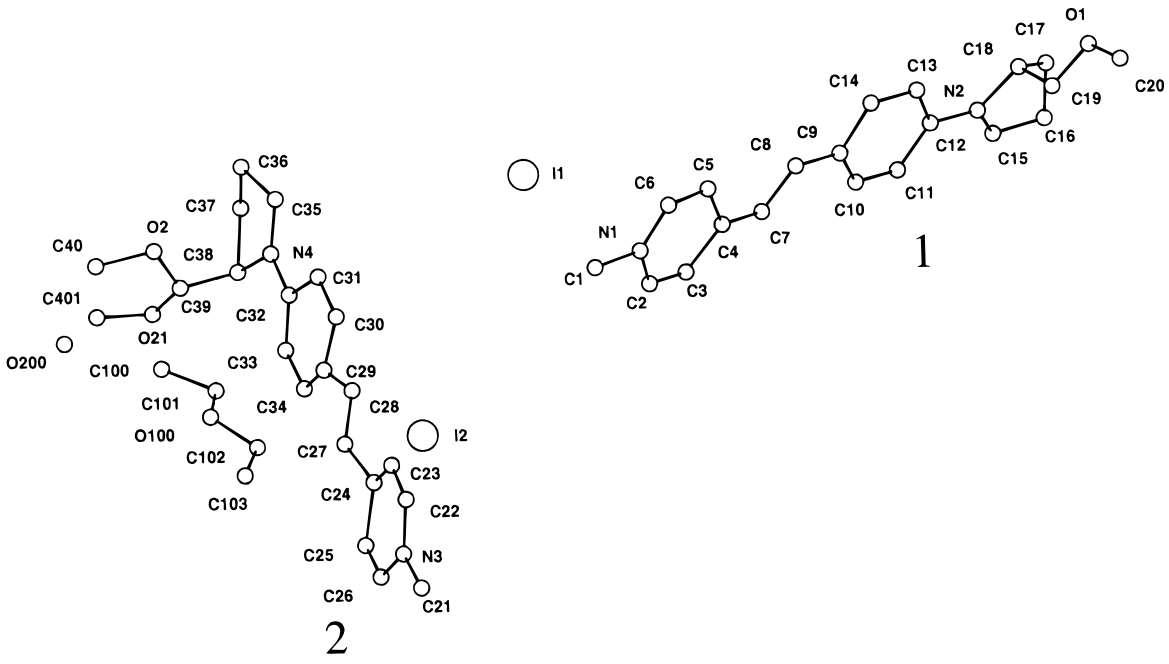

Figure 1. Atom labeling scheme for $MPMS^+I^-$·1/4 Et_2O·1/2 H_2O. H atoms are omitted for clarity.

Results and Discussion

Description of the Structure of $MPMS^+I^-$. Figure 1 illustrates the atomic numbering scheme employed in the asymmetric unit. It consists on two $MPMS^+$ cations (molecule 1, N(1), N(2), O(1), C(1)−C(20); molecule 2, N(3), N(4), O(2), O(21), C(21)−C(40), C(401)), two I^- anions, one-quarter of a diethyl ether molecule and one-half of a water molecule. The structure is made of discrete entities with no atoms in a special position. One $MPMS^+$ cation refers to another by a helicoidal 2_1 axis along *b*, which makes four cationic entities in the crystal cell. Disorder has been treated on the terminal methoxy group from molecule 2. It has not been necessary in case of molecule 1.

The main point of interest about the molecular structure concerns the true extent of the π-system involved in the intramolecular charge transfer and hence in the NLO response. The N(1)−N(2) and N(3)−N(4) linkage for molecules 1 and 2, respectively, which are expected to play a major role in the charge transfer as in the case for the analogous $DAMS^+$ cation, can be described as being roughly planar with the largest deviation of 0.21 and 0.28 Å observed at N(2) and C(28) atoms, respectively. Therefore all atoms located in the DAMS part of $MPMS^+$ are expected to be involved in the frontier orbital description.

No evidence for modifications of the electronic properties is expected in the substitution of the dimethylamino groups in $DAMS^+$ for the 2-(methoxymethyl)pyrrolidinyl cycle in $MPMS^+$. Anyway, this substituent is of prime importance to provide noncentrosymmetric material because of the presence of asymmetric carbons C(18) and C(38) for molecules 1 and 2, respectively, in the 2-(methoxymethyl)pyrrolidinyl cycle.

In $DAMS^+I^-$, the N^+-I^- distance between cations and anions is equal to 3.824 Å. In $MPMS^+I^-$, the N(1)−I(1) distance is 3.727 Å (molecule 1) and a distance of 3.874 Å is observed between N(3) and the I(2) anion generated by the symmetry operation $1 - x, -1.5 + y, 1 - z$ (molecule 2). In all instances, the iodide lies above the plane of the pyridinium rings. Therefore the local geometry may be considered as equivalent for the cation−anion pairs.

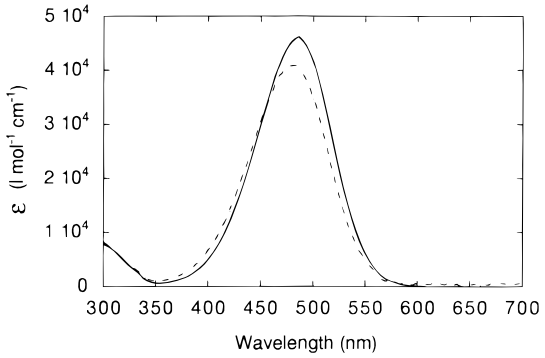

Figure 2. Electronic spectrum of $MPMS^+I^-$ recorded in EtOH. $DAMS^+I^-$ (dotted line) is shown as a reference.

Before discussing the SHG efficiency of $MPMS^+I^-$, it is interesting to compare the second-order NLO properties of the new $MPMS^+$ chromophore versus those of the well-known $DAMS^+$-related molecule.[12,22,34,35] The UV−visible spectra of $MPMS^+I^-$ and $DAMS^+I^-$ recorded in ethanol are compared in Figure 2. It can be easily observed that both chromophores exhibit a similar intense, low-lying transition located at 484 nm (ϵ = 46200 mol^{-1} cm^{-1}) and 481 nm (ϵ = 40 800 mol^{-1} cm^{-1}) for $MPMS^+I^-$ and $DAMS^+I^-$, respectively. In addition, the energy maxima (λ_{max}) of both chromophores recorded in solvent of different polarities are compared in Table 3. The data reveal that both compounds exhibit strong negative solvatochromism (red shift as the solvent polarity is decreasing). This behavior is usually associated with a decrease of the dipole moment upon excita-

(34) Marder, S. R.; Perry, J. W.; Schaefer, W. P. *Science* **1989**, *245*, 626.
(35) Bruce, D. W.; Denning, R. G.; Grayson, M.; Le Lagadec, Lai, K. K.; Pickup, B. T.; Thornton, A. *Adv. Mater. Opt. Electron.* **1994**, *4*, 293.

Table 2. Atomic Coordinates ($\times 10^4$) and Equivalent Isotropic Displacement Parameters (Å^2 $\times$ 10^3) for MPMS$^+$I$^-$[a]

	x/a	*y/b*	*z/c*	*U*(eq)
I1	9134(1)	6950(5)	5806(1)	74(1)
I2	4301(1)	6917(6)	6097(1)	80(1)
		Molecule 1		
N1	8472(17)	4540(4)	4333(12)	76(7)
N2	7770(2)	18610(5)	1704(13)	99(8)
C1	8640(2)	2520(4)	4685(15)	92(10)
C2	7690(2)	5280(7)	4165(16)	89(10)
C3	7479(18)	7080(10)	3878(14)	90(9)
C4	8090(2)	8210(5)	3673(14)	69(7)
C5	8930(2)	7440(4)	3896(16)	71(8)
C6	9050(2)	5630(5)	4200(14)	64(7)
C7	7870(2)	10160(5)	3363(13)	69(7)
C8	8418(19)	11400(6)	3181(14)	82(11)
C9	8230(2)	13230(6)	2822(17)	83(10)
C10	7440(2)	14310(5)	2613(14)	77(8)
C11	7260(2)	16050(5)	2272(13)	83(9)
C12	7912(19)	16980(11)	2097(11)	90(8)
C13	8750(2)	15980(5)	2295(14)	86(8)
C14	8900(2)	14330(6)	2679(17)	102(11)
C15	7040(3)	19860(6)	1519(18)	108(11)
C16	7040(3)	21150(7)	1081(19)	135(16)
C17	7960(3)	21500(6)	1225(18)	125(11)
C18	8390(3)	19460(6)	1432(15)	97(8)
C19	8470(3)	17890(6)	996(14)	97(10)
C20	9230(2)	17080(13)	359(16)	147(18)
O1	9060(2)	18690(5)	766(13)	133(11)
		Molecule 2		
N3	6522(14)	-10360(4)	5460(9)	54(5)
N4	8213(19)	3940(5)	8057(12)	90(7)
C21	6420(3)	−12360(5)	5125(13)	101(11)
C22	7252(19)	-9330(5)	5617(15)	62(7)
C23	7400(2)	−7550(6)	5910(17)	85(11)
C24	6830(3)	−6600(5)	6069(17)	91(10)
C25	5970(2)	−7730(10)	5944(14)	96(13)
C26	5880(2)	−9570(5)	5647(16)	75(8)
C27	7010(4)	−4660(7)	6520(2)	150(18)
C28	7470(2)	−2620(6)	6663(14)	88(9)
C29	7550(2)	−1590(6)	7033(14)	70(7)
C30	8280(2)	−600(6)	7089(14)	81(8)
C31	8530(2)	1220(4)	7438(14)	79(8)
C32	7940(16)	2140(8)	7705(9)	64(7)
C33	7140(2)	1320(6)	7561(14)	85(10)
C34	6920(2)	−520(6)	7209(16)	93(10)
C35	9000(3)	4780(6)	8189(18)	116(11)
C36	9110(4)	6550(12)	8680(2)	170(2)
C37	8250(3)	6990(11)	8579(14)	144(13)
C38	7630(3)	4810(6)	8363(16)	110(9)
C39	7620(2)	3460(8)	8858(19)	136(13)
C40	8240(4)	2250(14)	9730(2)	90(3)
C401	7234(9)	2540(2)	9584(6)	230(6)
O2	8380(3)	3020(8)	9213(19)	90(16)
O21	7020(5)	3840(14)	9070(3)	220(4)
O200	5796(9)	6180(2)	9939(6)	63(6)
C100	5245(9)	6950(2)	8917(6)	180(4)
C101	5166(9)	5920(2)	8282(6)	120(2)
O100	5165(9)	4010(2)	8205(6)	89(11)
C102	4913(9)	3010(2)	7622(6)	100(2)
C103	4920(9)	910(2)	7605(6)	88(16)

[a] Esd values in parentheses refer to the last significant digit. *U*(eq) is defined as the arithmetic mean of U_{ii}

tion ($\mu_e < \mu_g$) due to the stabilization of highly polar forms in the ground state. Large dipole moment changes ($\Delta\mu$) between the ground and the first excited states are strongly indicative of large second-order optical nonlinearities. This property has been suggested as a possible method for determining molecular hyperpolarizabilities.[36] The careful examination of the data gathered in

Table 3. Absorption Maxima (λ_{max} in nm) of the Lowest Energy Optical Transition for DAMS$^+$I$^-$ and MPMS$^+$I$^-$, in Solvents of Different Polarities

	DAMS$^+$I$^-$	MPMS$^+$I$^-$	E_TN[a]
$CHCl_3$	504	508	0.259
pyridine	493	500	0.293
EtOH	481	484	0.654
MeOH	475	480	0.765
MeCN	471	478	0.472
H_2O	449	460	1.000

[a] Reichardt empirical solvent parameter (ref 37).

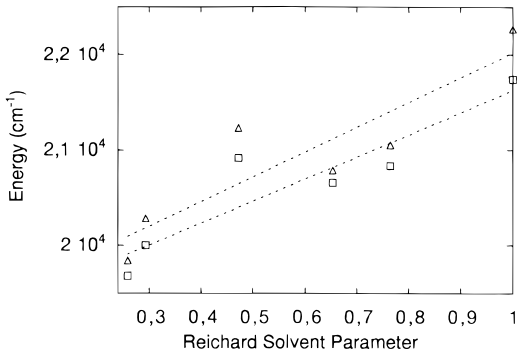

Figure 3. Energy maxima (cm^{-1}) versus the Reichardt solvent parameter (ref 37) for MPMS$^+$ (squares) and DAMS$^+$ (triangles). The slopes are indicative of similar $\Delta\mu$ for both chromophores.

Table 3 strongly indicates a similar extend for this behavior, as suggested in Figure 3, where the energy maxima are plotted versus the Reichardt solvent parameter.[37] The assumption that $\Delta\lambda$ is representative of $\Delta\mu$ can be made, taking into account the structural similarities between MPMS$^+$ and DAMS$^+$ (e.g. same π-electron framework). Figure 3 indicates that $\Delta\mu$ is in the same range of magnitude, with slopes equal to 2322 and 2609, for MPMS$^+$ and DAMS$^+$, respectively. In conclusion, the low-lying optical transitions of both chromophores roughly exhibit similar energies (E), slightly red shifted for MPMS$^+$, with slightly increased intensity (ϵ or oscillator strength),[38] and similar dipole moment changes ($\Delta\mu$). Therefore, within the framework of the two-level model (vide infra), spectroscopic evidence is provided for a slight enhancement of the hyperpolarizability, with $\beta_{MPMS^+} \approx 1.1\beta_{DAMS^+}$.

More evidence for similar hyperpolarizabilities between MPMS$^+$ and DAMS$^+$ is provided by theoretical calculations. The β values of MPMS$^+$ and DAMS$^+$ are reported in Table 4. As anticipated from the electronic spectra, the data reveal a slight enhancement of β for MPMS$^+$, with a different value for each molecule of the unit cell, probably due to the different molecular environment in the solid state. The averaged trend is in accordance with $\beta_{MPMS^+} \approx 1.2\beta_{DAMS^+}$, which is a little larger than expected from the above spectroscopic studies. The table indicates the well-known tendency for β enhancement when the second harmonic is close to the absorption maxima. The values of the hyperpolarizabilities at 1.064 μm, strongly enhanced by resonance, are not relevant; therefore, they are not

(36) Paley, M. S.; Harris, J. M.; Looser, H.; Baumert, J. C.; Bjorklund, G. C.; Jundt, D.; Twieg, R. J. *J. Org. Chem.* **1989**, *54*, 3774.

(37) Reichardt, C.; Harbush-Görnet, E. *Liebigs Annal. Chem.* **1983**, *5*, 721.

(38) Orchin, M.; Jaffé, H. H. *Symmetry Orbitals, and Spectra*; John Wiley: New York, 1971; p 204.

Table 4. Molecular Hyperpolarizability ($\beta_{Tot} = \beta_{2L} + \beta_{3L}$)[a] Calculated at Different Laser Frequencies for DAMS$^+$ and MPMS$^+$

	hyperpolarizability (10^{-30} cm^5 esu^{-1})					
			MPMS$^+$			
wavelength	DAMS$^+$		molecule 1		molecule 2	
(μm)	β_{tot}	($\beta_{2L} + \beta_{3L}$)	β_{tot}	($\beta_{2L} + \beta_{3L}$)	β_{tot}	($\beta_{2L} + \beta_{3L}$)
∞	−111	(−194 + 84)	-150	(−226 + 78)	-127	(−201 + 75)
1.907	−162	(−263 + 102)	-239	(−337 + 99)	-194	(−286 + 93)

[a] β is the total intrinsic quadratic hyperpolarizability = $(\beta_{x^2} + \beta_{y^2} + \beta_{z^2})^{1/2}$.

Table 5. Energies (λ_{Max} in nm), Oscillator Strength (f), Dipole Moment Changes between Ground and Excited State ($\Delta\mu$ in D), and Composition of the First Excited State of DAMS$^+$ and MPMS$^+$

compound		transition	λ_{max}	f	$\Delta\mu$	composition[a] of CI expansion
DAMS$^+$I$^-$		1 → 2	477	1.11	-17.5	0.937 $\chi_{46\rightarrow47}$
MPMS$^+$I$^-$	(1)	1 → 2	520	1.49	-12.2	0.958 $\chi_{60\rightarrow61}$
	(2)	1 → 2	500	1.55	-11.7	0.947 $\chi_{60\rightarrow61}$

[a] Orbital 46 is the HOMO, and 47 is the LUMO in DAMS$^+$. Orbital 60 is the HOMO, and 61 is the LUMO in MPMS$^+$.

reported in the table. Within the framework of the SOS perturbation theory, the molecular hyperpolarizability can be related to all excited states of the molecule and can be partitioned into two contributions, so-called two-level (β_{2L}) and three-level (β_{3L}) terms.[39] Analysis of term contributions to the molecular hyperpolarizability of MPMS$^+$I$^-$ and DAMS$^+$I$^-$ indicates that, in both cases, two-level terms dominate the nonlinearity, and can be related to the 1 → 2 low-lying electronic transition. It has long been recognized that this longest wavelength absorption band is responsible for the second-order NLO response of disubstituted stilbene and stilbazole derivatives, according to the well-known and widely used "two-level model".[40] In this model, the hyperpolarizability (β) can be described in terms of a ground and a first excited-state having charge-transfer character and is related to the energy of the optical transition (E), its oscillator strength (f), and the difference between ground and excited-state dipole moment ($\Delta\mu$) through the relation

$$\beta = \frac{3e^2\hbar f\Delta\mu}{2mE^3} \times \frac{E^4}{(E^2 - (2\hbar\omega)^2)(E^2 - (\hbar\omega)^2)}$$

In this equation, $\hbar\omega$ is the energy of the incident laser beam. INDO calculated data are reported in Table 5 for the 1 → 2 low-lying transitions of MPMS$^+$I$^-$ and DAMS$^+$I$^-$. This transition is the only intense band (large oscillator strength), in good agreement with the electronic spectra. In addition, the table is consistent with the main experimental features (λ_{max}, f, $\Delta\mu$). It principally involves the HOMO → LUMO transition, as indicated by the composition of the configuration interaction. Both orbitals are shown in Figure 4 for MPMS$^+$ and DAMS$^+$. The alkyl fragment bearing the asymmetric carbon of MPMS$^+$ is slightly involved in these orbitals. It is therefore not surprising that both chromophores exhibit closely related molecular optical nonlinearities. As an extension of the above result, it can be inferred that any chromophore based on the DAMS$^+$ conjugated structure with a chiral alkyl group (e.g. HPMS$^+$) should exhibit the same NLO response, which will rise to different bulk susceptibility, depending on the nature of the chiral substituent.

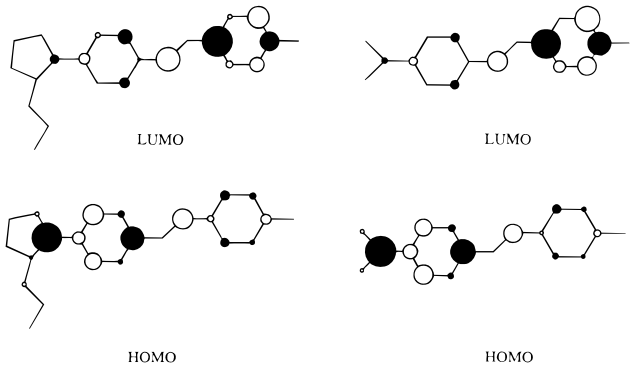

Figure 4. Comparison of HOMO and LUMO for MPMS$^+$ (left) and DAMS$^+$ (right) chromophores.

Table 6. SHG Efficiencies[a] Recorded at 1.907 μm

compounds	grain caliber (μm)	$I^{2\omega}$
urea	50−80	1
DAMS$^+$I$^-$		0
MPMS$^+$I$^-$	50−80	40
	80−125	65
	125−180	80
DAMS(TCNQ)$_2$		0
HPMS(TCNQ)$_2$		45[b]
MPMS(TCNQ)$_2$		0

[a] $I^{2\omega}$ relative to urea powder (reference). [b] Data from ref 15.

Bulk Efficiencies ($\chi^{(2)}$). The SHG efficiencies of the compounds investigated in this study are gathered in Table 6. As is well-known, the molecular nonlinearity associated with a chromophore (β) will lead to an observable bulk nonlinearity ($\chi^{(2)}$) only if this chromophore is oriented in a noncentrosymmetric environment.[41] DAMS$^+$I$^-$, which crystallizes in the centrosymmetric space group $P2_1/n$,[30] has an efficiency necessary equal to zero. However, the dipole moment and approximately linear shapes cause most of substituted stilbenes to crystallize in centrosymmetric space groups. Therefore, the zero efficiency recorded for DAMS(TCNQ)$_2$ is related to centrosymmetry of the crystal structure. The situation encountered for the MPMS$^+$ salts is expected to be different, as chirality provides the synthetic chemist with a means of guaranteeing that crystallization of a pure enantiomer will occur in a noncentrosymmetric point group. MPMS$^+$I$^-$ (chiral space group $P2_1$) exhibits a sizable NLO response (40−80 times that of urea) with phase matching. This situation, which implies that the efficiency is increasing with the size of the grains, is highly desirable for suitable NLO devices.

The relationship between microscopic and macroscopic second-order optical nonlinearities has been extensively investigated for any noncentrosymmetric crystal points group.[42] In the case of "push-pull" DAMS$^+$

(39) See for example: (a) Kanis, D. R.; Ratner, M. A.; Marks, T. J. *J. Am. Chem. Soc.* **1992**, *114*, 4, 10338. (b) Di Bella, S.; Fragalà, I.; Ledoux, I.; Marks, T. J. *J. Am. Chem. Soc.* **1995**, *117*, 9481.

(40) (a) Oudar, J. L.; Chemla, J. *J. Chem. Phys.* **1977**, *66*, 2664. (b) Oudar, J. L., *J. Chem. Phys.* **1977**, *67*, 446.

(41) Williams D. J., *Ang. Chem. Int. Ed. Engl.* **1984**, *23*, 690.

(42) Zyss, J.; Oudar, J. L. *Phys. Rev. A* **1982**, *26*, 2028.

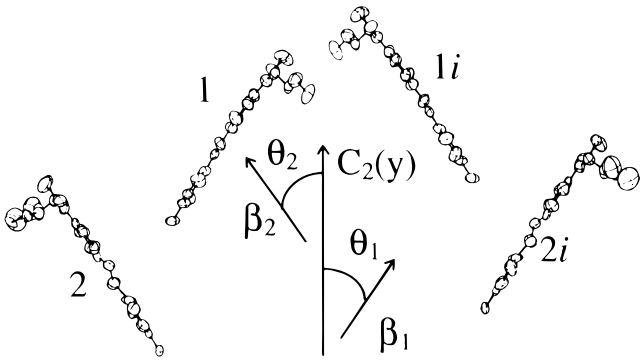

Figure 5. CAMERON view of $MPMS^{+-}$ showing the angles $\theta_1 = 33.65°$ and $\theta_2 = 37.15°$ between β_1 and β_2, respectively, for molecules 1 and 2, and the C_2 helicoidal axis (interaction i, symmetry operation $\bar{x}$, $y + 1/2$, $\bar{z}$).

derivatives, the only large hyperpolarizability tensor (β_{xxx}, along the charge-transfer axis x of the molecule) can be related to the corresponding crystalline first-order nonlinearity $\chi^{(2)}$ (components d_{IJK} in crystalline frame) through a relation, which, in space group $P2_1$ leads to

$$d_{YXX} = N f_Y^{2\omega} f_X^{\omega} f_X^{\omega} \beta_{xxx} \cos\theta \sin^2\theta$$

$$d_{YYY} = N f_Y^{2\omega} f_Y^{\omega} f_Y^{\omega} \beta_{xxx} \cos^3\theta$$

(N is the number of chromophores per unit volume, $f_I^{2\omega}$ and f_I^{ω} are Lorentz local-field factors, θ is defined as the angle between the main intramolecular charge-transfer axis ox and the 2-fold axis OY of the crystal). All other components of the tensor are neglectible. The optimization of d_{YYY} can be achieved with $\theta = 0°$, a situation which is of no use for birefringence phase matching and must therefore be avoided. More importantly, the angular factor weighting β_{xxx} in the expression of d_{YXX} is maximized and equal to 0.385 for $\theta = 54.74°$. Any phase-matching configuration emphasizing this coefficient is to be considered as highly desirable. The orientation of β in the crystal cell is shown in Figure 5 for $MPMS^+I^-$. θ is equal to 31.6° and 37.1° for the two chromophores present in the unit cell, which indicates that the orientation of the molecules is not optimized but corresponds to a sizable NLO answer.

As discussed above, the fact that a molecule is optically pure does not guarantee that the molecular packing will be optimized for NLO effects, but only that the chemist will ensure a noncentrosymmetric crystal structure. For instance, the charge-transfer system may set up a quasi-antiparallel geometry, thus canceling the major part of β, when θ is close to 90° in the above equations. Such an unexpected situation is that probably observed in $MPMS(TCNQ)_2$, which exhibits no observable SHG efficiency. This result is in great contrast versus the situation encountered for $HPMS(TCNQ)_2$, which exhibits SHG efficiency of 45 times that of urea.[15] (*S*)-(+)-2-Pyrrolidinemethanol, used in the synthesis of **5**, has already been successfully used for its simultaneous chiral and hydrogen-bonding character.[43] Without crystal structure, it can only be suggested

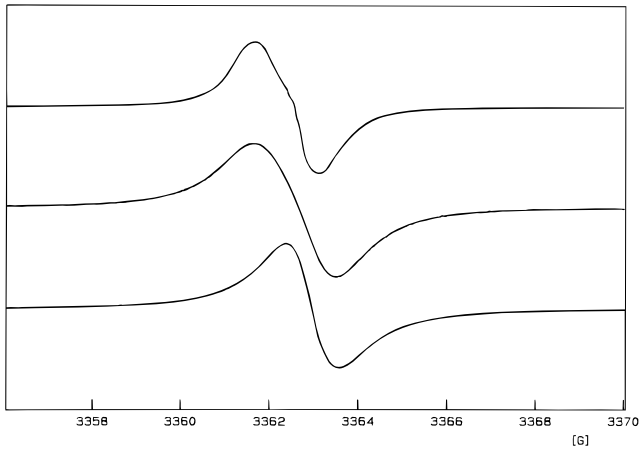

Figure 6. Powder X-band EPR spectra for $DAMS(TCNQ)_2$ (top), $MPMS(TCNQ)_2$ (middle), and $HPMS(TCNQ)_2$ (bottom).

that the chromophores are embodied very differently in $HPMS(TCNQ)_2$, due to hydrogen-bonding networks. Different intermolecular interactions probably result in different packing, which, as will be discussed below, can affect not only the NLO response, but the electronic properties of the TCNQ counterpart as well.

Electronic Properties of TCNQ Salts. The synthesis of the TCNQ salts reported in this study follows a general route which implies the reduction of $TCNQ^0$ by iodide, according to the equation:

$$2TCNQ^0 + C^+I^- \rightarrow C^+(TCNQ_2)^- + {}^1/_2I_2$$

where C^+ stands for $DAMS^+$ (**2**), $MPMS^+$ (**4**), and $HPMS^+$ (**5**). The reliability of elemental analysis is questionnable for the TCNQ salts of chiral $MPMS^+$ and $HPMS^+$ cations (especially for $HPMS(TCNQ)_2$) and might tentatively be related to the presence of solvent. However, no evidence was found from thermal analysis (no loss in weight in the range 20−250 °C). We[44] and others[45] have already obtained such disagreements in elemental analysis for powdered samples of conducting salts based on TCNQ. The modest quality of the crystals and possible decomposition at the surface may account for the disagreement observed in elemental analysis. However, this effect is not observed for the well-shaped needles of $DAMS(TCNQ)_2$ species.

The point of interest concerning these mixed valence compounds is to determine whether the TCNQ moieties are equally charged or not, which in the former case would favor highly conducting behaviors, while localized electrons would most likely be magnetically coupled. ESR spectra are shown in Figure 6. They all exhibit similar features: a very sharp signal (1.5, 1.8, and 1.2 G for $DAMS(TCNQ)_2$, $MPMS(TCNQ)_2$ and $HPMS(TCNQ)_2$, respectively) ascribable to $TCNQ^-$ radical ions ($g = 2.003$) with no evidence for a triplet state (no fine structure or half-field transition). These features sug-

(43) Zyss, J.; Nicoud, J. F.; Coquillay, M. *J. Chem. Phys.* **1984**, *81*, 4160.

(44) (a) Lacroix, P. G.; Daran, J.-C. *J. Chem. Soc., Dalton Trans.* **1997**, 1369. (b) Lacroix, P.; Kahn, O.; Valade, L.; Cassoux, P.; Thompson, L. K. *Synth. Met.* **1990**, *39*, 81.

(45) See for example: (a) Inoue, M. B.; Inoue, M. *Chem. Phys. Lett.* **1981**, *80*, 585. (b) Kunkeler, P. J.; P. van Koningsbruggen, P. J.; Cornelissen, J. P.; van der Horst, A. N.; van der Kraan, A. M.; Spek, A. L.; Haasnoot, J. G.; Reedijk, J. *J. Am. Chem. Soc.* **1996**, *118*, 2190. (c) Gross-Lannert, R.; Kaim, W.; Olbricht-Deussner, B. *Inorg. Chem.* **1990**, *29*, 5046.

Table 7. Bu-50 Mode[a] of TCNQ in C(TCNQ)$_2$, C$^+$ = DAMS$^+$ (2), MPMS$^+$ (4), HPMS$^+$ (5), Compared to Those of TCNQ^0 and TCNQ$^-$

C(TCNQ)$_2$	energy (cm^{-1})	references	energy (cm^{-1})
2	809 (m)	TCNQ^0	863
	832 (s)	TCNQ$^-$	828
4	810 (w)		
	832 (s)		
5	817 (w)		
	829 (m)		
	835 (s)		
	863 (w)		

[a] The vibrational mode of TCNQ is numbered according to ref 47.

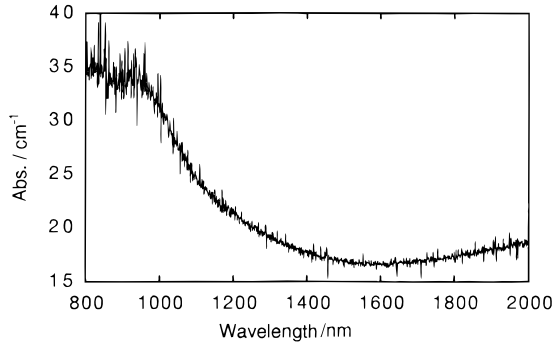

Figure 7. Electronic spectra and absorption (absorbance/thickness) in KBr pellets for HPMS(TCNQ)$_2$ showing the range of transparency in the near-IR domain. The thickness of the samples is about 0.4 mm.

gest some electron mobility. More precisely, several IR vibrational modes shift largely, depending on the charge occupation. TCNQ^0 and TCNQ$^-$ exhibit B_u-50 mode (CH bend) at 863 and 828 cm^{-1}, respectively, in a frequency domain where the materials are transparent enough to allow the energy to be determined precisely.[46,47] IR modes are shown in Table 7. The absence of the band at 863 cm^{-1} in DAMS$^+$(TCNQ)$_2$ and MPMS$^+$(TCNQ)$_2$ seems to indicate that no TCNQ^0 contaminates the materials that might be made of single species of TCNQ carrying a fractional charge. HPMS$^+$(TCNQ)$_2$ seems to be a little different, with a weak band at 863 cm^{-1}, which could suggest that, even if the electrons are not strictly pinned on single TCNQ$^-$, this compound exhibits a tendency for higher charge localization.

A representative electronic spectrum in a KBr pellet is shown in Figure 7, which indicates the range of transparency for these hybrid materials. These spectra can provide more evidence for the origin and magnitude of charge transfers observed in TCNQ salts. Following the early work of Torrance,[48] it has been well-established that transitions located in the near-IR (1500 to well beyond 2500 nm) arise from (TCNQ$^-$)(TCNQ^0) → (TCNQ^0)(TCNQ$^-$).[49−51] This provides a key to understanding the electronic structure and conductivity. Conductivities recorded on powder samples and intermolecular charge-transfer transitions are gathered in Table 8. The values are in the range 10^{-3}−10^{-2} Ω^{-1} cm^{-1}. In the absence of suitable crystals, extrinsic conductivities may significantly affect the data, although they were found to be reproducible over many samples. However, in agreement with IR spectroscopy, the data is consistent with a higher charge delocalization as the optical transition is shifted at lower energy. MPMS$^+$ and HPMS$^+$ cation are not flat, due to the CH_2OCH_3 and CH_2OH substituents, respectively. On the basis of a careful structural study of donor−acceptor salts, Delhaes has related the steric hindrance to the compactness of the stacking and therefore to the overlap and the conductivity.[52] His study has shown that out of plane substituents could effect dramatically the conducting properties. This effect is not dominant in MPMS(TCNQ)$_2$, which exhibits conducting and NLO properties closely related to the parent DAMS(TCNQ)$_2$, but when combined with hydrogen bonding, this may account for the different properties recorded in HPMS(TCNQ)$_2$. Even if no crystal structure is available, it may be inferred that the chromophores are organized in dimeric or oligomeric cationic species, which are far from being flat in this latter material. These structural features may deeply affect the TCNQ stacks and consequently lower the conductivity and enlarge the range of transparency, a situation highly desirable, when optical properties have to be considered.

Table 8. Conducting Properties of C(TCNQ)$_2$, in Relation with Intermolecular Optical Transitions. C$^+$ = DAMS$^+$ (2), MPMS$^+$ (4), and HPMS$^+$ (5)

C$^+$	wavelength (nm)	powder conductivity (S cm^{-1})
2	2860	6.0×10^{-3}
4	3300	5.1×10^{-3}
5	2160	2.3×10^{-3}

Conclusion

MPMS$^+$I$^+$ is a new NLO material exhibiting an SHG efficiency of 80 times that of urea, with phase matching. MPMS$^+$ turns out to be very closely related to the parents HPMS$^+$ and DAMS$^+$. These cations can be successfully combined with TCNQ units. Although no crystal structure was obtained for these hybrid salts, we have provided a set of measurements (conductivity, SHG, and spectroscopy) which strongly suggest that tunable structures can be achieved in the solid state by virtue of a chiral center, which result in different NLO and conducting properties. In particular, HPMS(TCNQ)$_2$ simultaneously exhibits second-order optical nonlinearity and semiconducting behavior. These attempts are part of our general research effort aimed at extending the range of molecular conductors combining two interacting properties in the same crystal. We have previously reported on the key idea of using reducible NLO cation in order to manipulate light (β) with electricity (partial charge transfer).[18] The present contribution has pointed out the combined effects of chirality and hydrogen bonding to overpass the strong tendency for centrosymmetry observed in molecular conductors. The next

(46) Inoue, M.; Inoue, M. B. *J. Chem. Soc., Faraday Trans. 2* **1985**, *81*, 539.
(47) Bozio, R.; Zanon, I.; Girlando, A.; Pecile, C. *J. Chem. Soc., Faraday Trans. 2* **1978**, *74*, 235.
(48) Torrance, J. B.; Scott, B. A.; Kaufman, F. B., *Solid State Commun.* **1975**, *17*, 1369.
(49) (a) Yu, L. J. *Synth. Met.* **1991**, 1745. (b) Yu, L. J. *Synth. Met.* **1991**, 1751.
(50) (a) Schwartz, M.; Hatfield, W. E. *Inorg. Chem.* **1987**, *26*, 2823. (b) Schwartz, M.; Hatfield, W. E. *NATO ASI Ser., Ser. B* 1987, 168 (Org. Inorg. Low-Dimens. Cryst. Mater.) 345.
(51) (a) Bandrauk, A. D.; Ishii, K.; Truong, K. D.; Aubin, M.; Hanson, A. W. *J. Phys. Chem.* **1985**, *89*, 1478.
(52) Delhaes, P.; Keryer, G.; Gaultier, J.; Fabre, J. M.; Giral, L. J. *J. Chim. Phys. Phys.-Chim. Biol.* **1982**, *79*, 299.

step of our studies will be the design of reductible chiral NLO cations capable of π-overlap with the acceptors. Several ferrocene-based derivatives are currently under investigation.

Acknowledgment. R.A. thanks EEC Training and Mobility of Researchers Program for a postdoctoral fellowship.

Supporting Information Available: Tables of crystal data and structure refinement, atomic coordinates, anisotropic displacement parameters, bond lengths and angles, and hydrogen atom positions, and structure factors for MPMS. The material is available free of charge via the Internet at http://pubs.acs.org.

CM9810436